forum acusticum 2026
8-12 September · Graz, Austria

A DEEP NEURAL NETWORK FOR PREDICTING THE SOUND FIELD RADIATED BY ORTHOGONALLY STIFFENED PLATES

Manuele Montrasio[1], Giacomo Squicciarini[2], Felix Langfeldt[2], Filippo Maria Fazi[2], Ivano La Paglia[1], Francesco Ripamonti[1], Roberto Corradi[1], Pietro Massini[3], Paola Caotti[3]

[1] *Department of Mechanical Engineering, Politecnico di Milano, Via G. La Masa 1, Milano 20156, Italy*
[2] *Institute of Sound and Vibration Research, University of Southampton, Southampton, SO17 1BJ, United Kingdom*
[3] *Product Development Audio System, ASK Industries S.p.A., Viale delle Officine Meccaniche Reggiane 1/F, Reggio Emilia 42124, Italy*

This paper is a revised version of the authors' submitted manuscript that was peer-reviewed by at least two anonymous reviewers.

Abstract

In recent years, the adoption of surrogate modeling in vibroacoustics applications is being explored. Artificial Neural Networks (ANNs) are proving their effectiveness in predicting structural vibration, and more recently their capabilities in sound radiation prediction is being investigating as well, paving the way for new research in the field. This paper explores the use of a Deep Neural Network (DNN) approach for the prediction of the sound field of plates with one orthogonal stiffener. In particular, the surrogate model can estimate the Sound Pressure Level (SPL) over a hemispherical surface enclosing a baffled plate of fixed dimensions, where the position of the stiffener and the forcing point is changed. The dataset for the network training is generated by numerical simulations combining FEM, Rayleigh integral and modal superposition. The results prove this approach to be promising and effective for tackling complex vibroacoustic problems.

Keywords: *Deep Neural Network, Sound Field Prediction, Orthogonally Stiffened Plate*

1. Introduction

Surrogate models are becoming increasingly popular for substituting complex numerical models, because of their ability to drastically decrease the computational effort. This is particularly useful when they are included in optimization algorithms, which usually require the computation of a large number of cases, and therefore efficiency becomes of paramount importance. The drawback of surrogate models is usually related to the accuracy of the prediction, which depends on the needs of the specific application and can be tuned to a desired level as a trade off with model complexity. Among all the different kinds of surrogate models, Neural Networks (NNs) have emerged as an efficient tool for addressing vibroacoustic problems. One of the most investigated applications in the field is the prediction of structural vibrations, for which different studies have proven the effectiveness of the approach. Cai and Jelovica [1] employed a Graph Neural Network (GNN) to predict stress distributions in stiffened plates with varying geometries. Seba and Kebdani [2] proposed a predictive model based on an Artificial Neural Network (ANN) to identify changes in the mechanical and geometric properties of composite plates with eccentric cutouts based on natural frequency. Van Delden et al. [3] developed a new network architecture, named Frequency-Query Operator, which predicts the vibration pattern of a plate with grooves, given a specific excitation frequency.

Few studies focus on the prediction of sound radiation of vibrating structures, with limitations regarding the frequency range and the number of evaluation points. To the best of the authors' knowledge, the closest example is the work by Longo et al. [4] that focuses on archtop guitars, where a neural network was used to predict natural frequencies, mobility and the Sound Pressure Level (SPL) in a single point in space, and restricting the evaluation to the first 5 eigenfrequencies.

However, recent studies demonstrate that more complex network architectures allow to extend the prediction to a broader frequency range and a larger number of sound radiation evaluation points. In particular, a major role is played by Physics-Informed Neural Networks (PINNs), which have recently obtained promising results. Zhou et al. [5] developed a

Corresponding author: *manuele.montrasio@polimi.it.*

PINN that predicts coupled structural vibrations and radiated sound pressure fields for rail transit bridge girders, achieving high accuracy across thousands of acoustic evaluation positions and over 2000 frequency points. Chen et al. [6] propose a PINN method for region-to-region sound field reconstruction.
Additional confirmation comes from the field of antennas: Singh et al. [7] included a surrogate model based on a neural network with transposed convolutional 2D layers inside an optimization algorithm. The network can successfully predict the electromagnetic radiation pattern at different frequencies generated by antennas with different geometries, which represents an application comparable to the prediction of sound radiation.
This work investigates potentials and limitations of this approach considering the specific case study of a rectangular flat plate with stiffeners, which is a typical choice in vibroacoustic problems [8], [9], [10]. Indeed, stiffeners are able to drastically change natural frequencies and mode shapes of a structure, while preserving a simple geometry, which is ideal for generating a challenging yet easy to set up test case. We propose a deep neural network based on fully connected layers and transposed convolutional 2D layers, that can predict the SPL in a specified frequency range of interest, for a set of evaluation points arranged on a hemisphere over a flat rectangular stiffened plate enclosed in a rigid baffle.

2. Materials, Models and Methods

In this section, a description of the proposed modelling strategy is reported. Specifically, in Section 2.1 the parametric numerical model of the plate with stiffeners used for the dataset generation is described. Later, Section 2.2 presents the development of the neural network, including the dataset generation, the neural network architecture and the training process.

2.1. Numerical Model

The case study considered in this work is a rectangular plate with fixed dimensions where the position of one stiffener is changed. The stiffener can be orthogonal to both the plate's edges and it runs through the entire length of the plate, as shown in Fig. 1. The case of a plate with no stiffeners is also considered. The position of the forcing point is another parameter of the model, which is highlighted in Fig. 1 as a red dot. The plate is excited by a harmonic point force perpendicular to the plate, with 1 N magnitude.
The computation of the sound radiation is performed in two steps. The structural vibration is first computed in COMSOL Multiphysics using a Finite Element (FE) simulation; then, the sound radiation of the baffled plate is evaluated in MATLAB through a method that combines Rayleigh integral and modal superposition approach, as described in the following subsections.

2.1.1. Structural Vibration

The dimensions and structural properties of the considered plate are shown in Table 1. The surface dimensions resemble an A5 paper sheet, in view of future

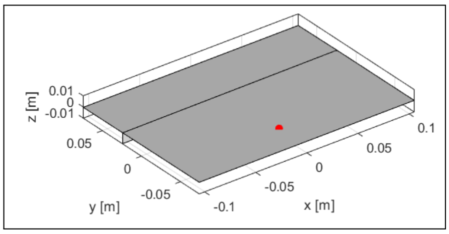

Figure 1: Geometry of a generic orthogonally stiffened plate with forcing point (red dot).

experimental validation. The stiffener height is tuned so as to significantly affect the mode shapes of the plate, yet avoiding its own bending modes in the $0-3000$ Hz frequency range considered in this work. The chosen material for both the plate and the stiffener is nylon and the material properties are taken from the corresponding built-in COMSOL material database. Both the plate and the stiffener are defined as thin shells, following the Mindlin-Reissner theory. The edges of the plate are clamped. For the mesh, a maximum element size of 5 mm was chosen, determined by a convergence analysis of the average mobility on various plates configurations with different stiffener and forcing point positions. The model performs an *Eigenfrequency Study* for a plate with given stiffener position, to compute the first 50 undamped eigenfrequencies and mode shapes, determined from a convergence study on sound radiation related Frequency Response Functions (FRFs). Damping contribution is accounted in the computation of sound radiation, introduced as loss factor η, and whose value is indicated in Table 1.

Table 1: Structural properties and baseline geometrical parameters of the plate.

Parameter	Symbol	Value
Young's Modulus	E_p	2 GPa
Poisson's Ratio	ν_p	0.4
Density	ρ_p	1150 kg/m^3
Loss factor	η	0.01
plate length	l_p	0.210 m
plate width	w_p	0.148 m
plate thickness	t_p	0.002 m
Stiffener height	h_s	0.010 m
Stiffener thickness	t_s	0.002 m

2.1.2. Sound Radiation

To compute the sound radiation, a method that combines the Rayleigh integral and the modal superposition approach is used [11]. This method allows reducing the computational effort, compared to the standard Rayleigh integral computed at each frequency of the considered range.
For a harmonic point force at coordinates $\mathbf{x}_F = (x_F, y_F)$ and angular frequency ω, the modal velocity

amplitude is given by

$$u_n(\mathbf{x}_F) = \frac{\mathrm{j}\omega F \phi_n(\mathbf{x}_F)}{[\omega_n^2(1+\mathrm{j}\eta) - \omega^2]M_n}, \quad (1)$$

where n indicates the eigenfrequency index, ϕ_n is the *n-th* undamped mode shape, ω_n is the *n-th* natural frequency, M_n is the *n-th* modal mass, F is the force amplitude and η is the loss factor.
The complex velocity field of the plate can be obtained through the modal superposition approach as

$$v(\mathbf{x}) = \sum_{n=1}^{\infty} u_n(\mathbf{x}_F)\phi_n(\mathbf{x}), \quad (2)$$

where $\mathbf{x} = (x, y)$ is an arbitrary point on the surface. Starting from the complex plate velocity $v(\mathbf{x})$, the Rayleigh integral provides the complex acoustic pressure radiated from a baffled flat surface at any arbitrary position in space $\mathbf{r} = (r, \theta, \varphi)$

$$p(\mathbf{r}) = \frac{\mathrm{j}k\rho_0 c}{2\pi} \int_S v(\mathbf{x}) \frac{\mathrm{e}^{-\mathrm{j}kr'}}{r'} \mathrm{d}\mathbf{x}, \quad (3)$$

where k is the acoustic wavenumber and $r' = |\mathbf{r} - \mathbf{x}|$ represents the distance between a point $\mathbf{x}$ on the plate surface and a point in space at $\mathbf{r} = (r, \theta, \varphi)$.
By combining Eq. (2) and Eq. (3) the following expression can be derived

$$p(\mathbf{r}) = \sum_{n=1}^{\infty} u_n(\mathbf{x}_F) A_n(\mathbf{r}), \quad (4)$$

where $A_n(\mathbf{r})$ is defined as

$$A_n(\mathbf{r}) = \frac{\mathrm{j}k\rho_0 c}{2\pi} \int_S \phi_n(\mathbf{x}) \frac{\mathrm{e}^{-\mathrm{j}kr'}}{r'} \mathrm{d}\mathbf{x}. \quad (5)$$

Eq. (4) represents the modal superposition in the acoustic domain, and it allows to compute the complex pressure at any arbitrary position in space $\mathbf{r}$. The parameters characterizing the equations above are reported in Table 2.
The proposed method is then solved numerically, considering a finite summation including 50 eigenfrequencies in Eq. (4), and considering the surface integral as a summation of discrete surface elements in Eq. (5). A convergence analysis was adopted to define the dimension of the surface elements, which led to a maximum element size of 5 mm. The acoustic pressure is then evaluated on a sampled hemisphere with radius of 0.5 m, shown in Fig. 2. The azimuth coordinate is sampled with resolution $\Delta\varphi = 20°$, while the elevation coordinate resolution is $\Delta\theta = 10°$. The total number of evaluation points is 162. This spatial resolution allows to have an acceptable accuracy in the frequency range of interest when performing spatial interpolation with spherical harmonics, as it has been verified through a convergence analysis.

Table 2: Values of the parameters used for the sound radiation computation.

Parameter	Symbol	Value
Air density	ρ_0	1.225 kg/m^3
Speed of sound	c	343 m/s
Force amplitude	F	1 N

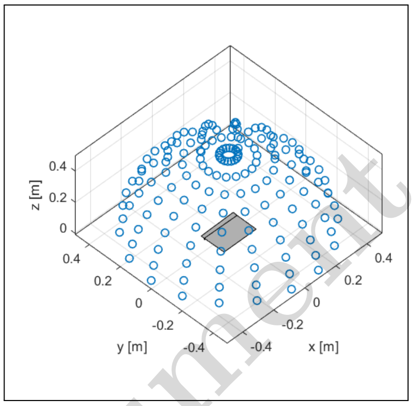

Figure 2: Set of acoustic pressure pressure evaluation points, sampled on a hemisphere enclosing the baffled plate.

2.2. Neural Network

2.2.1. Neural Network Architecture

The proposed neural network architecture is shown in Fig. 3. It was inspired by the one proposed by Singh et al. [7] for the prediction of electromagnetic radiation from parameterized antenna designs. The network includes two main parts: an encoder and a decoder. The encoder is composed of fully connected layers with ReLu activation functions. Its main role is to increase the dimensionality of the input vector to reach the so called *Latent Vector*, which matches the dimension of the output vector. The *Latent Vector* is then reshaped to a 3D matrix of suitable size (dimensions 9x18x256, see Fig. 3), which represents the input of the decoder. The decoder is composed of transposed convolutional 2D layers with ReLu activation functions, batch normalization and kernel size of 4. This representation of the data helps the network in modeling the relationships between adjacent SPL values in space and frequency. Finally, the output vector is obtained by reshaping the 3D matrix into a 1D vector. The total number of learnables in the proposed neural network architecture is 7.4 million.
In the next section, more details about inputs and outputs will be provided and the dataset generation procedure will be described.

2.2.2. Dataset Generation and Training

The dataset is generated according to the processing chain described in Section 2.1. The input vector consists of 4 real values: the x and y coordinates of the stiffeners respectively parallel to the y- and x-axis, and the x and y coordinates of the excitation

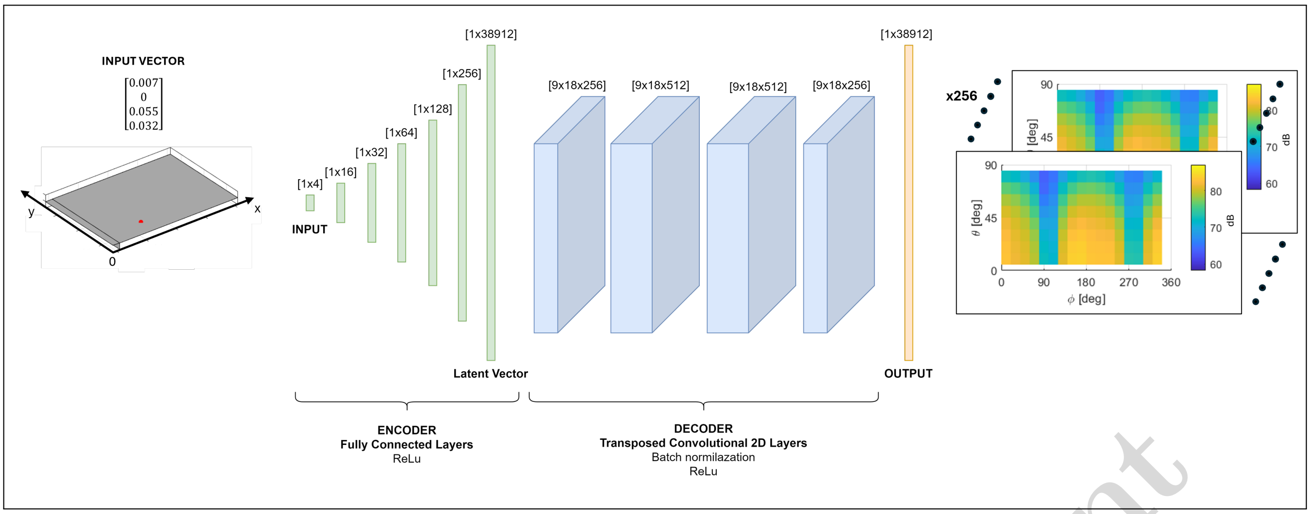

Figure 3: Architecture of the proposed neural network.

point. The origin of the reference system is defined in the bottom left corner of the plate (see Fig. 3), and the position of both stiffener and the excitation point is limited to be at least 5 mm from the edges of the plate. The configuration without a stiffener is represented by setting both stiffeners coordinates to zero. The dataset dimension is set to 8000 samples for each combination of stiffener orientation, namely no stiffeners (0x0), one stiffener parallel to the x-axis (0x1) and one stiffener parallel to the y-axis (1x0), resulting in a total dataset dimension of 24000 samples. Latin Hypercube Sampling [12] is used separately for each combination of stiffener orientation. The output vector is composed of the SPL matrices for each evaluated frequency, reshaped into a 1D vector (Fig. 3). As a first attempt, the frequency range is defined from 500 to 2200 Hz, with a resolution of 400 points per decade to ensure sufficient accuracy in capturing the resonance peaks of the FRFs. This range includes multiple natural vibration modes and yields a total of 256 frequency points, a power of two that enables more efficient computation. This led to a total dimension of the output vector of 38912. Note that the lower and upper frequencies are arbitrarily set within the 0-3000 Hz range defined by the numerical model, as explained in Section 2.1.

Input and output vectors are normalized using z-score normalization. The dataset is randomly divided in 70% training, 15% validation and 15% test. The training is carried out using the ADAM optimizer, L2 regularization and MSE loss function. The training parameters are reported in Table 3 and the network's dimensions (i.e. number of layers and number of neurons) are reported in Fig. 3. All hyperparameters have been empirically chosen by testing different configurations.

3. Results and Discussion

The neural network is effective in reducing the computational effort and time, which is reduced by a factor of 20 when compared to the numerical model used for the dataset generation and described in Section 2.1. As a reference, on the same machine, the computation time to perform the calculation of the sound radiation for a single case for the specified frequency range, reduces from about 10 s to 0.5 s. This can be quite beneficial in contexts like optimization algorithms, where multiple cases need to be computed.

Table 3: Training parameters.

Parameter	Value
Mini-Batch Size	128
Initial Learning Rate	1×10^{-3}
Dropout Rate	0.5
Learning Rate Drop Period	50
Early Stopping	40
Kernel size	4

The overall prediction performance is evaluated through the Mean Square Error (MSE), the Root MSE (RMSE) and the de-normalized RMSE, which are shown in Table 4. The latter is calculated after the output is de-normalized according to the z-score normalization used to pre-process the dataset. The training error is lower than the validation and test errors, but they are still similar enough to exclude the occurrence of overfitting during training. The de-normalized RMSE provides us an indication on the overall average error in dB, which can be considered satisfactory, given that it is between 1.5 and 1.6 dB for the three datasets.

Randomly selected prediction results for a plate from the test dataset, which is unseen by the network during training, are shown in Fig. 4. The plate geometry and excitation location are shown in Fig. 4a. Fig. 4b shows the comparison between the ground truth SPL, obtained using the numerical model described in Section 2.1, and predicted SPL at one specific evaluation

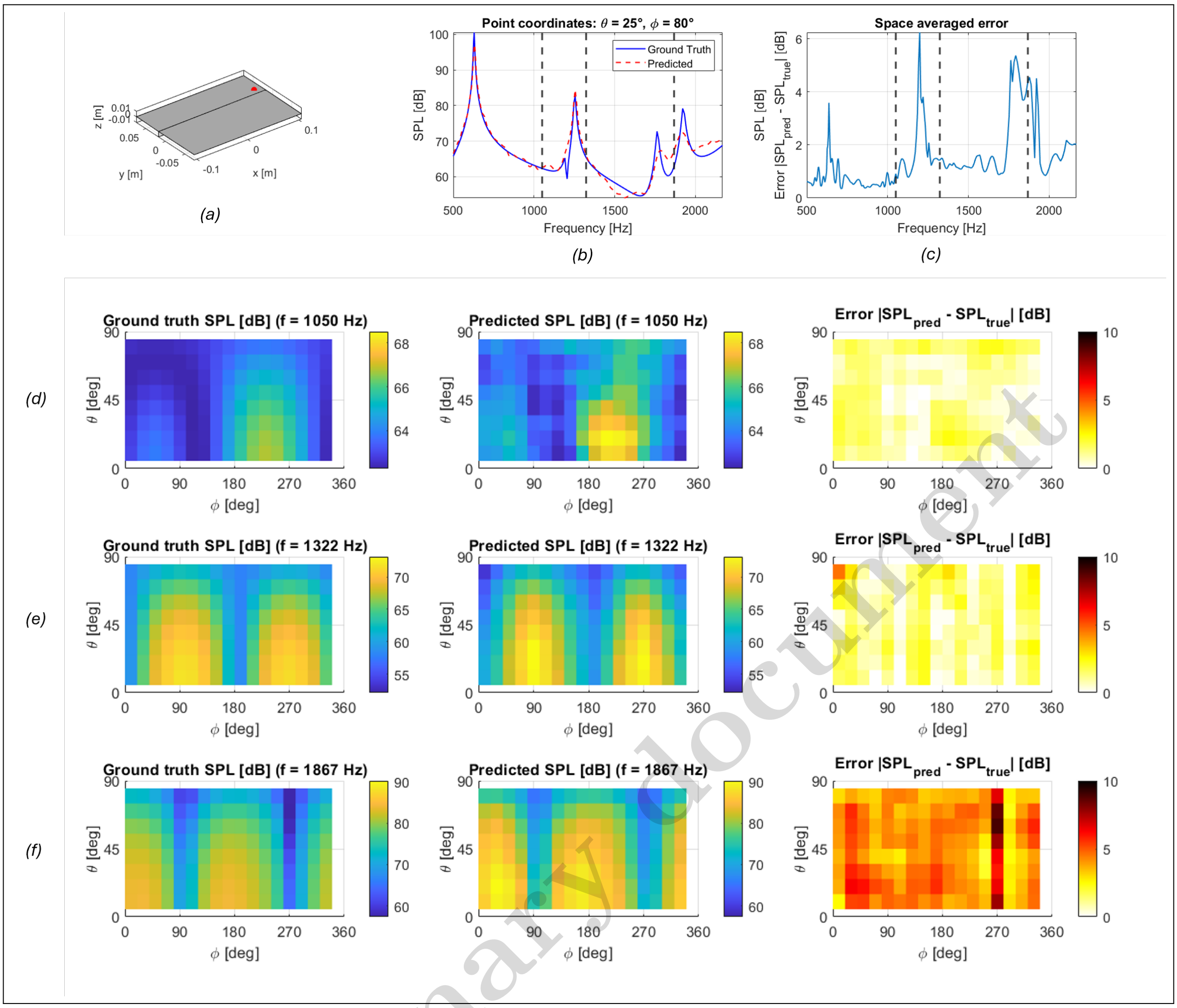

Figure 4: Prediction results for a plate configuration from the test set. *(a)* Geometry. *(b)* Comparison between ground truth and predicted SPL at one specific evaluation point, as a function of frequency. *(c)* Error in SPL prediction averaged over the evaluation points, as a function of frequency. *(d)(e)(f)* Ground truth SPL, predicted SPL and error over the entire set of evaluation points, for three arbitrary frequencies indicated as dashed vertical lines in *(b)*.

Table 4: Performance metrics for the neural network on training, validation, and test sets.

Dataset	MSE	RMSE	De-n. RMSE
Training	0.0158	0.1257	1.5004
Validation	0.0172	0.1310	1.5632
Test	0.0172	0.1310	1.5662

point, as a function of frequency. The error is calculated as the absolute value of the difference between the two. In Fig. 4c, the error averaged over all 162 evaluation points as a function of frequency is shown. For most frequencies the error is below 2 dB, while it increases in correspondence of resonance peaks, especially when multiple resonances are close to each other in terms of frequency. Additionally, the results for all the evaluation points at three selected frequencies are shown in Fig. 4d, Fig. 4e and Fig. 4f. Each row refers to one frequency, which is also indicated as a vertical dashed line in the upper plots. The columns show, from left to right, the ground truth SPL, the predicted SPL and the error. Here the neural network performance is appreciated in terms of the prediction of the radiation pattern. Indeed, even when the error is high, as it is in the last case, the pattern is accurately predicted by the network, which makes it effective in applications where directivity is important.
As a final remark, the network's ability to generalize beyond the training case, with respect to variations in material properties, boundary conditions and geometry, was not investigated in this work. Nevertheless, such an analysis is necessary for a comprehensive as-

sessment of the network's capabilities, and it should be addressed in future studies.

4. Conclusions

This paper presented results of a study on the capabilities of a neural network to predict the sound field radiated by orthogonally stiffened plates. The model is derived adopting a deep neural network architecture, trained considering different positions of both the stiffener and the force exciting the plate. For this first analysis, a simple test case of a plate with one stiffener excited by a point force is considered. The neural network aims at predicting the SPL over a set of evaluation points sampled on a hemisphere over the baffled plate.

The results are satisfactory, as the network successfully predicts the sound radiation of plates not included in the training dataset with a spatially averaged error lower than 2 dB over most of the frequencies. In addition, the prediction of the radiation pattern is consistently accurate, even at those frequencies characterized by higher errors in SPL amplitude. This makes the network particularly effective when the focus is on the directivity of the radiated sound.

Future developments of this work include the extension to multiple stiffeners, which will add complexity to the problem and is expected to require adjustment in terms of the network architecture and dataset dimension.

5. Acknowledgments

This study is carried out in the framework of a cooperation agreement between Politecnico di Milano and ASK Industries S.p.A. The authors gratefully acknowledge ASK Industries S.p.A. for providing support and valuable contribution to the research project.

References

[1] Y. Cai and J. Jelovica, *Graph Neural Network for Stress Predictions in Stiffened Panels Under Uniform Loading*, Sep. 2023. DOI: 10.48550/arXiv.2309.13022. arXiv: 2309.13022 [cs]. Accessed: Nov. 14, 2025.

[2] M. R. Seba and S. Kebdani, "Finite Element and Neural Network Based Predictive Model to Determine Natural Frequency of Laminated Composite Plates with Eccentric Cutouts under Free Vibration," *Advances in Technology Innovation*, vol. 7, no. 2, pp. 131–142, Mar. 2022, ISSN: 2518-2994, 2415-0436. DOI: 10.46604/aiti.2022.8909. Accessed: Nov. 14, 2025.

[3] J. van Delden, J. Schultz, C. Blech, S. C. Langer, and T. Lüddecke, *Learning to Predict Structural Vibrations*, 2023. DOI: 10.48550/ARXIV.2310.05469. Accessed: Nov. 14, 2025.

[4] G. Longo, S. Gonzalez, F. Antonacci, and A. Sarti, "Predicting the Acoustics of Archtop Guitars using an AI-based Algorithm trained on FEM Simulations," in *Proceedings of the 10th Convention of the European Acoustics Association Forum Acusticum 2023*, Turin, Italy: European Acoustics Association, Jan. 2024, pp. 2965–2971, ISBN: 978-88-88942-67-4. DOI: 10.61782/fa.2023.0662. Accessed: Nov. 17, 2025.

[5] H. Zhou, X. Song, W. Luo, C. Cai, and L. Wu, "CASP-Net: A physics-informed neural network model for vibro-acoustic coupling analysis in rail transit bridge structures," *Journal of Sound and Vibration*, vol. 620, p. 119 481, Jan. 2026, ISSN: 0022460X. DOI: 10.1016/j.jsv.2025.119481. Accessed: Mar. 25, 2026.

[6] X. Chen, S. Zhao, F. Ma, E. Cheng, and I. S. Burnett, *Permutation-Invariant Physics-Informed Neural Network for Region-to-Region Sound Field Reconstruction*, 2026. DOI: 10.48550/ARXIV.2601.19491. Accessed: Jun. 12, 2026.

[7] P. Singh, S. S. Panda, J. C. Dash, B. Riscob, S. K. Pathak, and R. S. Hegde, "Rapid Multi-Objective Antenna Synthesis via Deep Neural Network Surrogate-Driven Evolutionary Optimization," *IEEE Journal on Multiscale and Multiphysics Computational Techniques*, vol. 10, pp. 151–159, 2025, ISSN: 2379-8815, 2379-8793. DOI: 10.1109/JMMCT.2025.3544270. Accessed: Nov. 17, 2025.

[8] C. Knuth, G. Squicciarini, and D. Thompson, "An Engineering Approach for Estimating the Radiation Efficiency of Orthogonally Stiffened Plates," *Journal of Vibration and Acoustics*, vol. 145, no. 3, p. 031 006, Jun. 2023. DOI: 10.1115/1.4056741.

[9] D. Zhao, N. S. Ferguson, and G. Squicciarini, "Acoustic response of thin-walled, orthogonally stiffened cylinders," *IOP Conference Series: Materials Science and Engineering*, vol. 657, no. 1, p. 012 007, Oct. 2019. DOI: 10.1088/1757-899X/657/1/012007.

[10] D. Zhao, G. Squicciarini, and N. Ferguson, "Vibroacoustic response of stiffened thin plates to incident sound," *Applied Acoustics*, vol. 172, p. 107 578, Jan. 2021. DOI: 10.1016/j.apacoust.2020.107578.

[11] G. Squicciarini, D. Thompson, and R. Corradi, "The effect of different combinations of boundary conditions on the average radiation efficiency of rectangular plates," *Journal of Sound and Vibration*, vol. 333, no. 17, pp. 3931–3948, Aug. 2014. DOI: 10.1016/j.jsv.2014.04.022.

[12] M. D. McKay, R. J. Beckman, and W. J. Conover, "A Comparison of Three Methods for Selecting Values of Input Variables in the Analysis of Output from a Computer Code," *Technometrics*, vol. 21, no. 2, p. 239, May 1979, ISSN: 00401706. DOI: 10.2307/1268522. JSTOR: 1268522. Accessed: Mar. 27, 2026.